Available online at www.sciencedirect.com
ScienceDirect
Tectonophysics 426 (2006) 263–279
TECTONOPHYSICS
www.elsevier.com/locate/tecto

Strike-slip motions in the Gulf of Siğaçik (western Turkey): Properties of the 17 October 2005 earthquake seismic sequence

Christoforos Benetatos [a], Anastasia Kiratzi [a,*], Athanassios Ganas [b], Maria Ziazia [b], Areti Plessa [b], George Drakatos [b]

[a] *Department of Geophysics, Aristotle University of Thessaloniki, 54124, Thessaloniki, Greece*
[b] *National Observatory of Athens, Geodynamics Institute, Athens 118 10, Greece*

Received 15 March 2006; received in revised form 25 July 2006; accepted 3 August 2006
Available online 26 September 2006

Abstract

The October 2005 series of earthquakes that occurred in the Gulf of Siğaçik (western Turkey) reveal the operation of pure strike-slip faults, as evidenced from the 49 focal mechanisms we determined, in a region dominated by N–S extension and bounded by well-documented graben structures. The sequence is characterized by the occurrence of three moderate size events (17 October 2005, 05:45 UTC, Mw 5.4; 17 October 2005, 09:46 UTC, Mw 5.8; and 20 October 2005, 21:40 UTC, Mw 5.8) with an eastward propagation and close spatial separation (<6 km). We relocated over 200 aftershocks, combining phases from the Greek and Turkish seismological networks, which align roughly in a NE–SW cloud, but considerably spread after the first day of the sequence, indicating the simultaneous activation of multiple structures nearly orthogonal to the main rupture. It is hard to relate the occurrence of the events to any of the previously mapped faults in the region. The region of occurrence is a well-known geothermal area which implies that it is in a very unstable state, with the fault systems close to rupture and very sensitive to stress perturbations. Here we showed that the sequence is adequately explained by static stress triggering. It is worth noting that this sequence, though moderate in magnitudes, provides stronger evidence for the operation of sub-parallel strike-slip faults in the central Aegean Sea–western Turkey, north of the volcanic arc, which seem to be optimally oriented in the regional stress field and facilitate the Anatolia motion into the Aegean Sea.

Keywords: Seferihisar; Siğaçik Gulf; Western Turkey; Aegean Sea; Focal mechanisms

1. Introduction

In October 2005 intense seismic activity burst in the Gulf of Siğaçik(district of Seferihisar) in western Turkey (rectangle in Fig. 1). The two strongest events of the sequence both had magnitudes equal to Mw 5.8, masking the identification of a classic mainshock, and occurred on 17 and 20 October, 2005 at 09:46 and 21:40 UTC, respectively. These events were preceded on 17 October 2005 at 05:45 by a Mw 5.4 earthquake. The nearby Chios and Samos Islands (Greece) and the cities of Izmir and Urla in Turkey were shaken, but no life loss was reported. Most of the damage was reported in the districts of Seferihisar and Urla.

The region of occurrence of these events is famous for its historical heritage, (Dewey and Sengör, 1979;

* Corresponding author. Tel.: +30 2310 998486; fax: +30 2310 998528.
E-mail address: kiratzi@geo.auth.gr (A. Kiratzi).

0040-1951/$ - see front matter © 2006 Elsevier B.V. All rights reserved.
doi:10.1016/j.tecto.2006.08.003

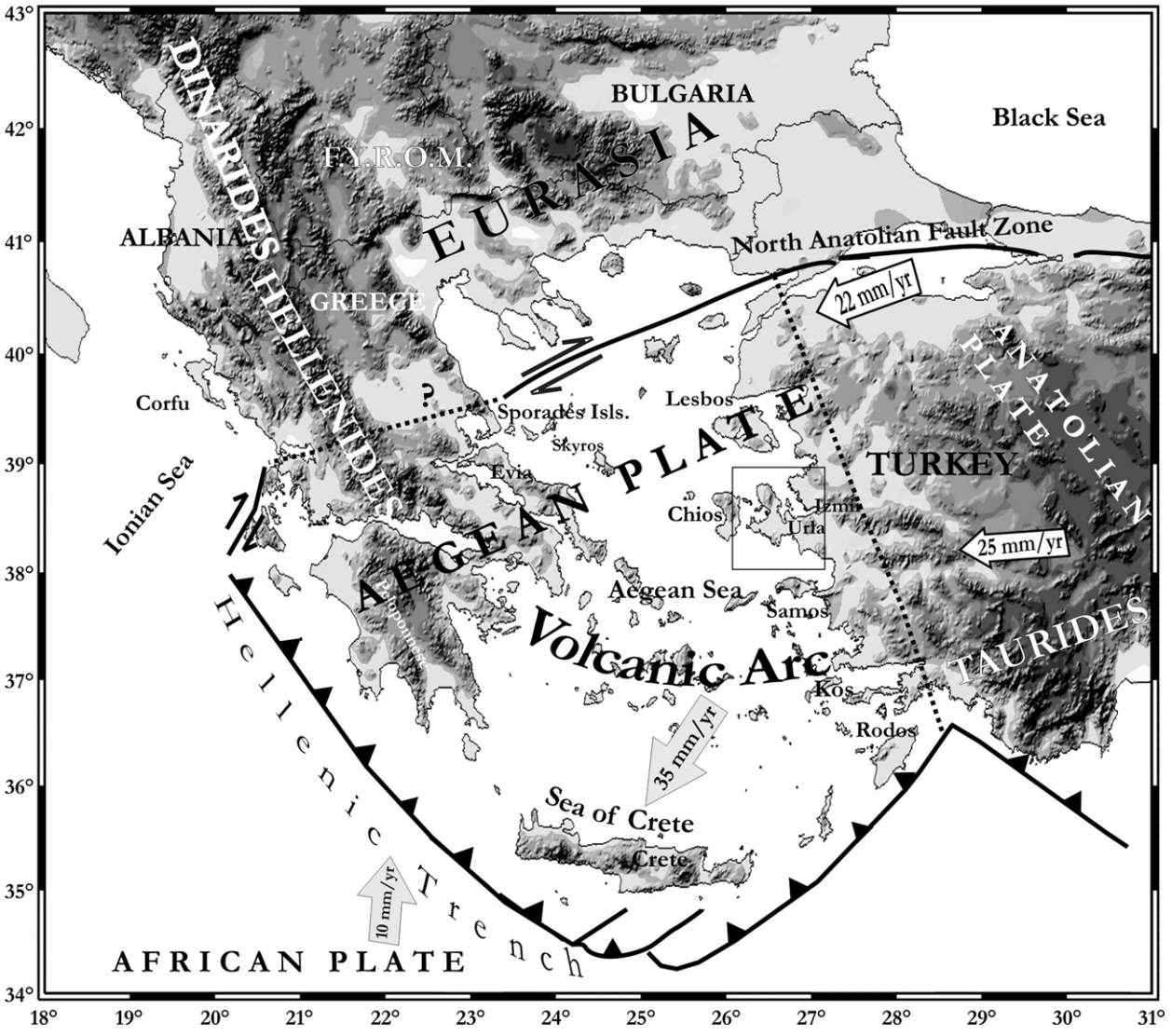

Fig. 1. Main features of the Aegean Sea and surrounding lands. Dashed lines mark the eastern and northern edges of the Aegean plate (as in Papazachos, 1999), and the rectangle indicates the region of occurrence of the 2005 in western Anatolia, located in the transition zone from the Anatolia to the east to the Aegean plate to the west, while arrows indicate the motion of the plates relative to Eurasia (McClusky et al., 2000).

Papazachos and Papazachou, 2002; Altinok et al., 2005) located in the western part of the Gediz and Menderes graben systems, and contains several normal faults, very prominent in the morphology, with an ~E–W strike (Dewey and Sengör, 1979). Of equal importance are the NE–SW and NW–SE trending faults which additionally play significant role on the tectonics (Yilmaz, 1997). In terms of plate motion models, the region belongs to the transition zone between two plates, of Anatolia plate in the east and of the Aegean plate in the west (Papazachos, 1999; McClusky et al., 2000). South of the North Anatolian Fault the plate motion of Anatolia relative to Europe can be adequately described by a simple rigid body rotation with a dominant E–W component and an average velocity of ~24 mm/yr (McClusky et al., 2000). The westward escape of Anatolia is facilitated by the low elevations in the Aegean Sea. The Aegean plate moves almost uniformly in a SSW direction with an average velocity of 35 mm/yr in the southern parts (McClusky et al., 2000). The change of Anatolia rotation to the Aegean translation occurs along the central and southern parts of western Turkey (Papazachos, 1999). The stress field is mainly extensional in a NNE–SSW direction combined with considerable strike-slip motions (Kiratzi, 2002; Koukouvelas and Aydin, 2002; Kiratzi and Louvari, 2003 and references therein).

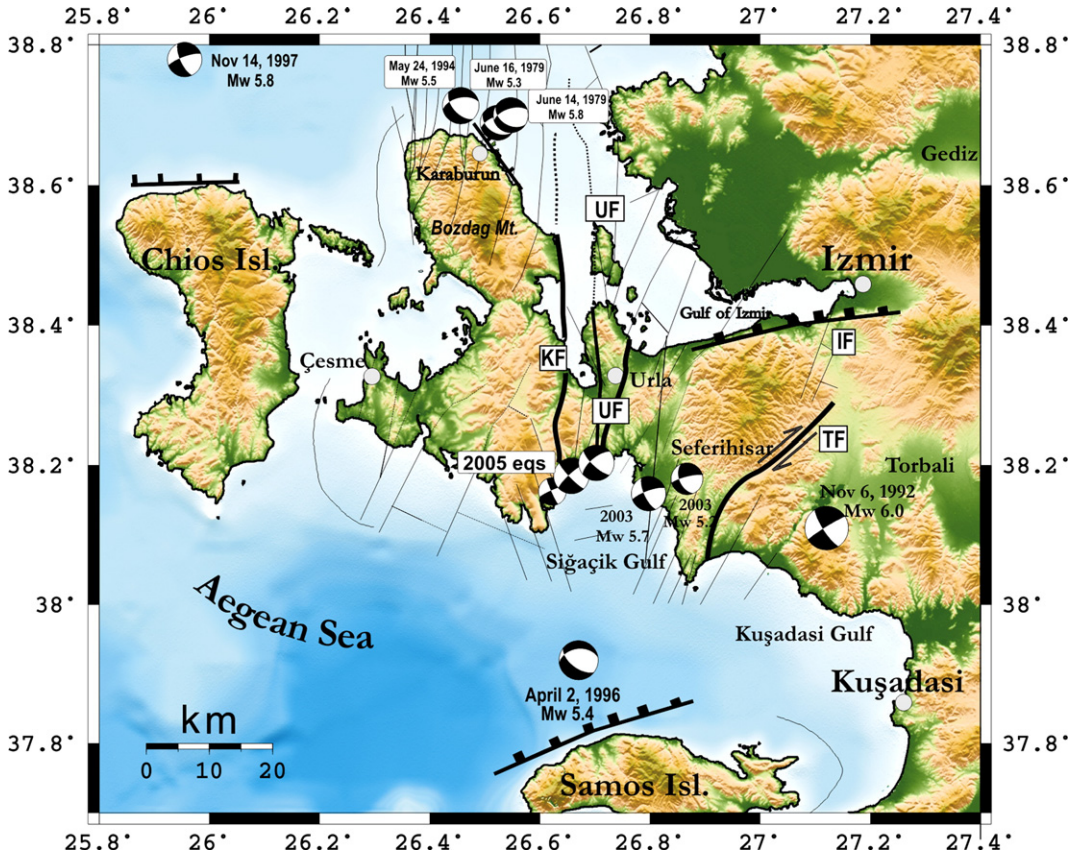

Fig. 2. Focal mechanisms of previous strong events (Table 1), together with those of the strongest events of the 2005 sequence (Table 2). Main structures clearly seen on morphology (from Ocakoğlu et al., 2004, 2005) are also plotted (KF = Karaburun Fault, UF = Urla Fault, TF = Tuzla Fault and IF = Izmir Fault). The focal mechanisms show pure strike-slip motions in the Gulf of Sığaçik and normal faulting combined with considerable strike-slip motion in the north (Karaburun peninsula) and in the south (near Samos Island).

Here we study the characteristics of the 2005 sequence, focusing on the distribution of aftershocks and of focal mechanisms in terms of the regional stress field, we discuss about the main fault ruptures, and we examine how the strongest events of the sequence affected the stress field in view of the general consensus that even small static stress changes due to the coseismic displacement can trigger off-fault earthquakes (Harris, 1998 and references therein).

2. Regional tectonics

Fig. 2 summarizes the most prominent tectonic structures which are marked on morphology (from Ocakoğlu

Table 1
The parameters of the focal mechanisms of previous strong events in the area (CMT Harvard solutions)

No	Date	Time	Lat° N	Lon° E	Depth km	Mw	Nodal Plane 1			Nodal Plane 2			*P* axis		*T* axis	
	Yr/m/day	Hh/mm/s					Strike	Dip	Rake	Strike	Dip	Rake	Az	Dip	Az	Dip
1	790614	11:44:46	38.74	26.50	15	5.8	253	59	−120	121	42	−50	112	63	4	9
2	790416	18:41:59	38.69	26.54	10	5.3	255	58	−124	127	45	−48	112	61	8	7
3	921106	19:08:10	38.09	27.19	25	6.0	238	85	−167	147	77	−5	103	13	12	6
4	940524	02:05:39	38.71	26.49	21	5.5	258	54	−135	138	55	−46	107	55	198	1
5	960402	07:59:24	37.92	26.67	15	5.4	262	41	−127	127	58	−62	87	65	198	9
6	971114	21:38:53	38.80	25.87	15	5.8	242	80	−156	148	67	−10	107	23	13	9
7	030410	00:40:16	38.17	26.76	15	5.7	250	76	−159	155	70	−15	114	24	22	4
8	030417	22:34:22	38.19	26.90	15	5.2	256	79	−139	156	50	−15	124	36	20	19

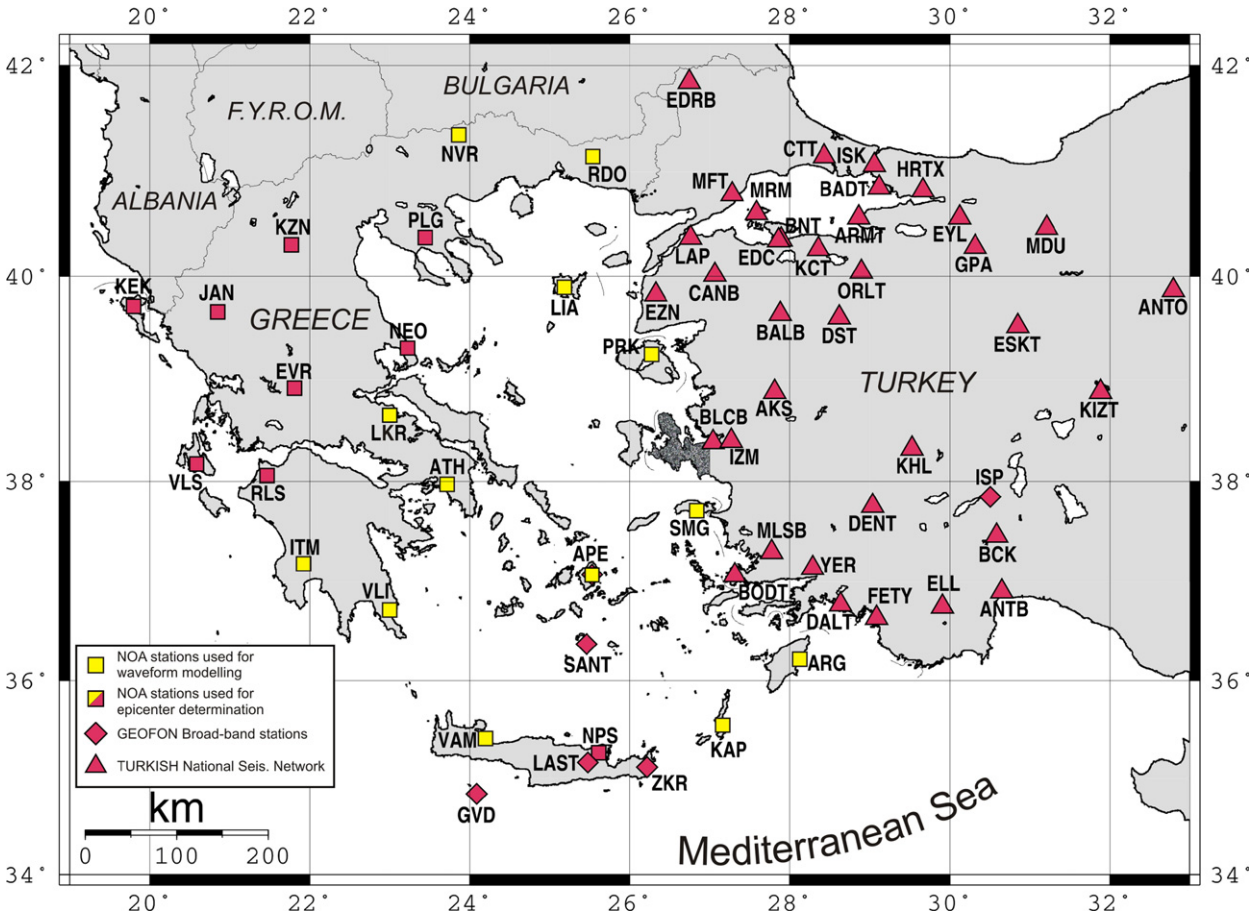

Fig. 3. Location of the stations whose records we used a) to locate epicentres (all stations) and b) to invert for the focal mechanism solutions (only records from NOA broad band stations marked with light coloured squares). (For interpretation of the references to colour in this figure legend, the reader is referred to the web version of this article.)

et al., 2004, 2005) together with the focal mechanisms of previous events (see Table 1 for details). Close spatial separation of strong contrasts in topography is observed, with the roughly north-south Bozdag mountain range (1212 m high), and the steep slopes falling directly into the sea. Focusing in the Seferihisar region the most prominent features are the Karaburun Fault (KF), the Urla Fault (UF), the Izmir Fault (IF) and the Tuzla Fault (TF). Recently (Ocakoğlu et al., 2004, 2005), based on multi-channel reflection data, identified: a) KF as an active reverse faulting, responsible for the raise of Karaburun peninsula; b) UF as an N–S trending reverse fault; c) stressed out the importance of strike-slip faulting in the region and d) mapped the continuation of active structures off-shore (also shown in Fig. 2 just to indicate the cross-cut pattern of faulting). The Izmir Fault is a normal fault bounding the southern Gulf of Izmir, and its activity has been well documented with the occurrence of strong events (e.g. 178 (6.5), 1040 (6.8), 1654 (6.4), 1680 (6.2), 1688 (6.8), 1723 (6.4), 1778 (6.4); Papazachos and Papazachou, 2002). The Tuzla Fault (~40 km in length) is a dextral strike-slip fault based on the offset of river channels and the focal mechanisms of recent events (Ocakoğlu et al., 2005 and references therein).

The most devastating earthquake in Urla district, from the historical period, is reported on 15 October 1883; Mw 6.8 (38.4° N, 26.6° E) which produced the destruction of 3600 houses and the death of 120 people in Urla and Çesme (Papazachos and Papazachou, 2002). For the instrumental period previous seismic activity in the broader Seferihisar region includes the earthquakes of 16 November 1992 (Mw 6.0) and of 10 April 2003 (Mw 5.7) which was followed on 17 April 2003 with an Mw 5.2 event. Both the 1992 (Scordilis et al., 1994) and 2003 events are connected with right-lateral strike-slip motions, based on the distribution of aftershocks which align in an ENE–WSW direction. The more distant, to the region of study, events, north of Karaburun peninsula

and north of Samos Island, have focal mechanisms that show normal faulting with strike-slip components, and the north dipping planes are probably the fault planes in all three cases (Papazachos and Papazachou, 2002).

3. Distribution of epicentres and focal mechanisms of the 2005 sequence

To locate the epicentres we combined P and S phases derived from the Greek and Turkish seismological stations (Fig. 3), e.g. the networks operated by the National Observatory of Athens (NOA) and by the Kandilli Observatory of Turkey. To determine the focal mechanisms of the strongest events of the sequence we used regional waveforms as recorded from the broad band sensors of NOA network.

3.1. Distribution of epicentres

We hand-picked P and S phases from the digital records of 3-component instruments from the NOA network, covering the period 17 October to 22 November 2005. We added the phases from the Turkish network as have been provided to us. The average number of phases used was 29, which was adequate enough for the location process, and we ended with 235 best located events with 12 or more phases. The closest seismological station of the NOA network is located on Samos Island (code SMG) at a distance of ~50 km from the sequence, while the closest station from the Turkish network is BLCB at a distance of ~35 km, contributing significantly to focal depth estimates. We used HYPOELLIPSE (Lahr, 1999) and after several tests with regional models we preferred to use the velocity model of Panagiotopoulos (1984) which has as follows: V_g=6 km/s, d_g=19 km; V_b=6.6 km/s, d_b=12 km, overlying a half-space with V_n=7.9 km/s (Fig. 4). This model has been tested in the past and has been extensively used for the routine earthquake locations in the broader Aegean Sea region. Here, it produced the smallest uncertainties in the locations compared to the model of Novotny et al. (2001) which we prefer to use for moment tensor inversions, based on previous experience (Roumelioti et al., 2003).

Fig. 5 (a to d) shows the distribution of the best located events, (distribution of location uncertainties also shown), and the evolution of the sequence in selected time windows. In the first 5 h following the occurrence of the 17 October Mw 5.4 earthquake, (Fig. 5a) the few aftershocks form a small cluster trending NE, where in its easternmost end the second strong Mw 5.8 event occurred almost 4 h later. (Fig. 5a). Approximately 19 h after the occurrence of the first event (Fig. 5b) the sequence develops in a NE–SW

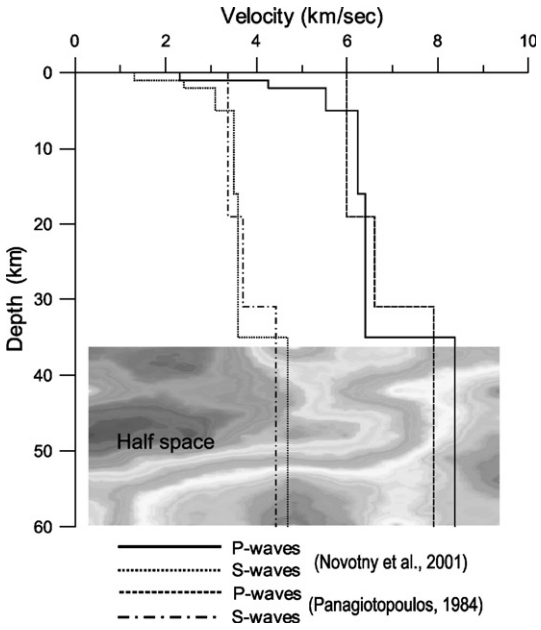

Fig. 4. Velocity models used for epicenter location (model of Panagiotopoulos, 1984) and for the regional waveform modelling (Novotny et al., 2001).

trend, while the activation of other structures orthogonal to this main trend is evident. The same pattern is also observed during the first 3 days (Fig. 5c), with the last strong event to occur again at the easternmost end of the activated area. The entire sequence (Fig. 5d) indicates that the activity is concentrated along the northern margin of the Gulf of Siğaçik, the trend of the aftershocks is NE–SW, and the activation of nearby small faults is evident. This pattern of off-fault aftershock activity is more clearly seen in the work of Aktar et al. (submitted for publication) who have installed a local network to monitor aftershocks. The accuracy of their locations clearly shows the activation of two main structures, one trending NW–SE bounding the western coast of the Gulf of Siğaçik and the other trending NE–SW, along the central coast of the Gulf. These two aftershock clouds are orthogonal to each other, forming conjugate strike-slip faulting.

The first Mw 5.4 event has a clearly defined directivity towards ENE (Benetatos et al., in preparation), which implies that the NE–SW nodal plane is the fault plane, and the sense of strike-slip motion is right lateral. The two Mw5.8 events occurred very close in space, have very similar focal mechanisms (Table 2) and their waveforms are strikingly similar (Fig. 6). Based on the directivity of the first event of the sequence, the relocation of the three strongest events, the evolution of the sequence mainly along a NE–SW trend and the regional tectonics, we conclude that the 2005 sequence implies the activation of

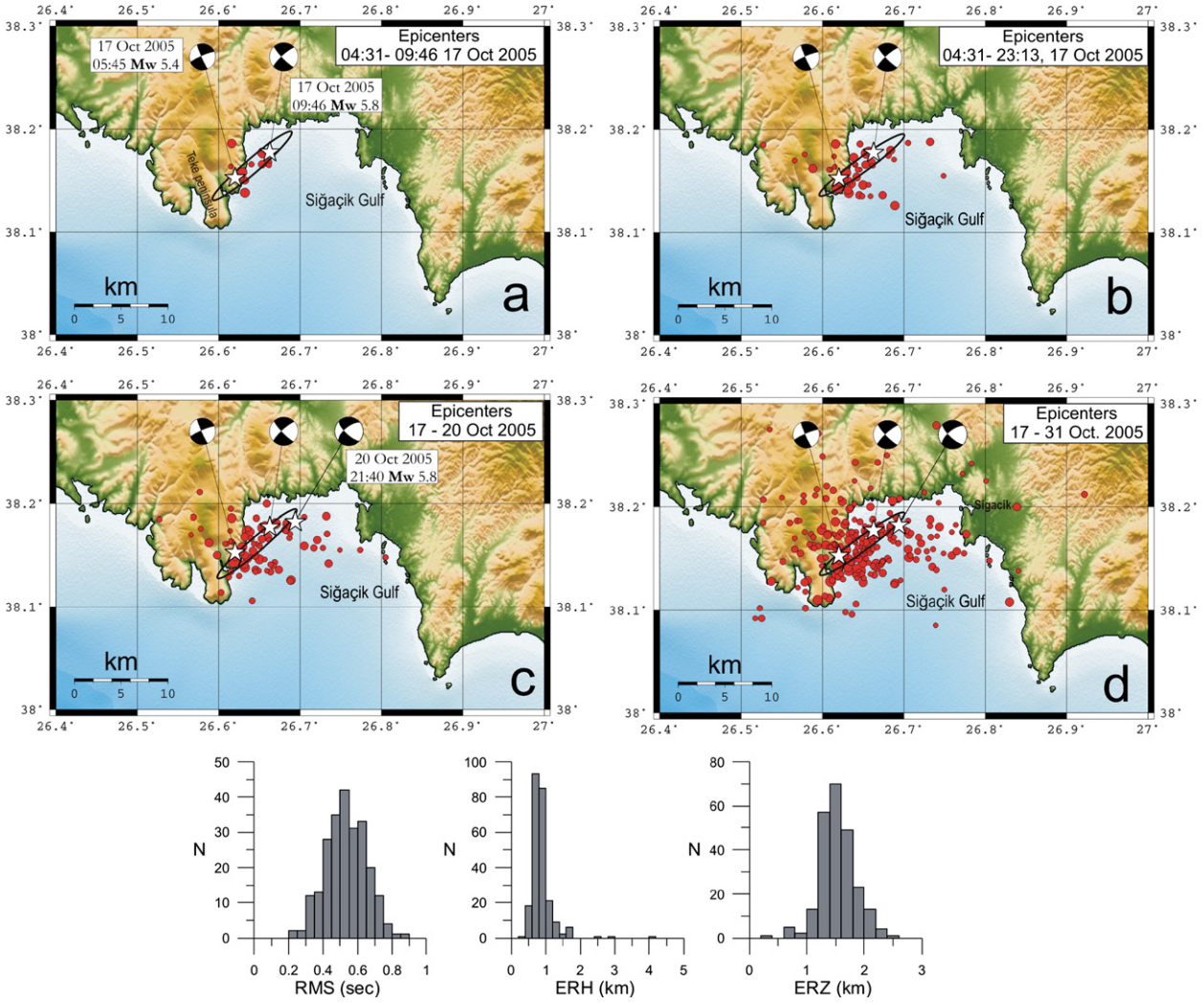

Fig. 5. Evolution of aftershock activity (circles) in selected time windows, in relation with the occurrence of the strongest events (stars) of the 2005 sequence, its approximate dimensions marked by the ellipse (for a Mw 5.8 earthquake). a) For the first 4 h until the occurrence of the 17 October 09:45, M 5.8 event b) of ~ the first day of 17 October, c) For 17 to 20 October 2005, d) All one-month aftershocks. Note the simultaneous activation of off-fault structures within the first 24 h. The uncertainties in epicentre locations are also shown in the lower part (Root Mean Square (RMS), Horizontal (ERH) and vertical (ERZ)).

a ENE–WSW trending dextral strike-slip fault. With the previous reasoning we also connect the three strongest events with the same rupture (ellipse in Fig. 5) which for an Mw 5.8 event the along strike-length is of the order of 10 km and the width is ~6.0 km (Wells and Coppersmith, 1994).The plethora of aftershocks observed off the main aftershock cloud can be treated as off-fault aftershocks, usually observed in aftershock sequences. Actually this part of western Turkey is a well-documented geothermal area (Drahor and Berge, 2006) and these areas are known to be unstable regions, with a fault system in a mechanical equilibrium state very close to rupture, as suggested by their high sensitivity to transient stress perturbations. This fact probably explains the diffuse pattern of aftershock activity and the simultaneous activation of many structures. The fault mapping of Ocakoğlu et al. (2004, 2005) already suggests a complex conjugate net of faults.

3.2. Distribution of focal mechanisms

We used the regional moment tensor inversion technique (Dreger and Helmberger, 1990, 1991, 1993) to determine the focal mechanisms for 49 events of the sequence. The method is routinely applied now and we do not go into detailed analysis (the reader can refer to Dreger, 2002 and references therein). Green's functions

Table 2
Parameters of the focal mechanisms of the October 2005 sequence that we determined using regional moment tensor inversion applied to broad band waveforms

No	Date	Time	Lat° N	Lon° E	Depth km	Mw	*N*	VR (%)	Nodal Plane 1			Nodal Plane 2			*P* axis		*T* axis	
	Yr/m/day	hh/mm/s							Strike°	Dip°	Rake°	Strike°	Dip°	Rake°	Az°	Dip°	Az°	Dip°
1	051017	04:31:27	38.150	26.632	10	3.9	4	71	157	70	−25	256	67	−158	116	31	207	2
2	051017	05:45:19	38.153	26.620	15	5.4	10	78	156	85	−8	247	82	−175	111	9	202	2
3	051017	06:16:07	38.168	26.660	12	3.9	2	69	156	74	−31	255	60	−162	112	33	208	9
4	051017	07:05:49	38.158	26.629	18	4.1	5	74	172	80	−17	265	73	−170	128	19	219	5
5	051017	07:49:52	38.164	26.615	6	3.6	1	47	166	58	−95	355	32	−82	62	76	259	13
6	051017	08:07:30	38.166	26.653	16	3.8	3	70	175	80	−12	267	78	−170	131	16	221	1
7	051017	08:28:54	38.177	26.654	18	4.3	6	76	161	81	−24	255	67	−170	116	23	210	10
8	051017	08:34:45	38.138	26.632	11	4.2	4	70	152	85	−43	247	47	−173	100	33	207	25
9	051017	08:50:04	38.166	26.640	5	3.4	1	35	221	85	−165	130	75	−5	86	14	355	7
10	051017	09:46:57	38.178	26.663	7	5.8	7	92	136	81	−11	228	79	−171	92	14	182	1
11	051017	09:55:32	38.147	26.635	21	5.2	4	63	164	85	−17	255	73	−175	118	15	211	8
12	051017	10:57:31	38.140	26.640	5	3.7	3	59	327	83	−10	59	80	−173	283	12	13	2
13	051017	11:20:27	38.180	26.684	6	3.9	4	77	145	82	−16	237	74	−172	100	17	192	6
14	051017	11:48:48	38.187	26.705	16	3.7	1	61	351	82	71	239	21	157	97	34	240	49
15	051017	12:02:23	38.152	26.753	5	3.4	1	62	141	86	18	49	72	176	274	10	6	16
16	051017	12:05:42	38.132	26.673	7	3.2	1	41	47	79	−24	142	66	−168	2	25	96	9
17	051017	12:09:54	38.175	26.681	4	3.5	2	63	153	81	−37	250	54	−168	105	32	207	18
18	051017	12:22:33	38.136	26.674	7	3.7	4	67	239	85	164	330	74	5	286	8	193	15
19	051017	12:32:03	38.146	26.657	6	3.2	1	56	251	72	−143	148	55	−22	115	39	16	11
20	051017	12:34:02	38.392	27.011	10	3.6	1	67	142	81	−39	239	52	−169	93	33	196	19
21	051017	12:43:30	38.146	26.650	8	4	3	88	319	83	10	227	80	173	93	2	183	12
22	051017	13:16:43	38.179	26.657	5	3.9	2	96	151	85	−29	244	61	−174	104	24	201	16
23	051017	13:22:51	38.173	26.638	11	3.8	4	59	155	83	−8	246	82	−173	110	11	201	1
24	051017	14:53:22	38.126	26.689	17	3.4	1	45	38	90	12	128	78	0	84	8	352	8
25	051017	23:13:17	38.154	26.642	10	3.9	5	78	249	88	174	340	84	2	295	3	204	6
26	051018	05:04:52	38.134	26.664	5	3.5	2	43	52	74	−164	317	75	−41	274	22	5	1
27	051018	16:00:49	38.174	26.635	22	4.2	4	66	167	82	35	71	55	103	294	18	35	30
28	051018	22:49:28	38.159	26.705	19	3.9	4	65	77	81	171	168	81	164	123	0	33	13
29	051019	05:51:24	38.129	26.612	17	3.6	2	51	176	88	−19	267	71	−86	130	15	223	12
30	051019	10:11:31	38.181	26.670	15	4.6	8	79	244	89	178	334	88	1	289	1	199	2
31	051019	10:22:34	38.168	26.632	7	3.7	2	63	332	86	36	239	54	175	100	21	202	28
32	051020	09:10:53	38.157	26.717	19	4	4	73	71	89	−179	341	89	−1	296	1	206	0
33	051020	21:40:04	38.183	26.694	7	5.8	7	92	133	73	−25	231	66	−162	90	30	183	5
34	051021	00:34:15	38.112	26.608	20	3.8	3	64	353	90	19	83	71	0	40	13	306	13
35	051021	11:47:38	38.178	26.599	10	4.3	7	77	244	88	−175	154	85	−2	109	5	19	2
36	051021	16:34:40	38.200	26.839	13	3.7	4	59	44	81	162	137	72	10	92	6	359	19
37	051022	07:21:03	38.157	26.765	12	3.7	4	50	151	87	−17	242	73	−176	105	14	198	10
38	051022	15:35:26	38.184	26.628	19	3.7	3	63	80	89	179	170	89	1	125	0	35	1
39	051022	18:00:08	38.185	26.560	20	3.6	2	46	338	82	46	240	45	169	101	24	210	37
40	051022	19:05:07	38.149	26.715	18	3.5	2	40	341	86	−10	72	80	−176	296	10	27	4
41	051023	14:59:38	38.110	26.594	17	4	7	80	79	88	171	169	81	2	124	5	34	8
42	051024	16:55:39	38.155	26.573	12	3.6	4	60	169	87	17	78	73	177	302	10	35	14
43	051024	17:03:17	38.092	26.525	18	3.6	2	60	239	81	142	336	53	11	293	18	191	32
44	051024	21:15:38	38.174	26.607	18	3.9	4	79	155	89	−4	245	86	−179	110	4	200	2
45	051025	08:58:27	38.178	26.702	20	3.8	3	75	163	86	23	71	67	175	295	13	29	19
46	051026	17:48:08	38.127	26.578	13	3.8	4	69	349	89	−17	79	73	−179	303	13	35	11
47	051029	14:48:42	38.128	26.610	14	4.2	4	70	162	70	−25	261	67	−158	121	31	212	2
48	051031	05:26:40	38.138	26.644	16	4.9	5	83	231	75	156	328	67	17	281	5	188	27
49	051031	06:48:22	38.127	26.650	12	4.2	4	79	340	88	−3	70	87	−178	295	4	25	1

N refers to the number of stations used for the calculation of the focal mechanism and VR (%) is the total variance reduction of the inversion.

were computed using the FKRPROG code (Saikia, 1994) using the velocity model of Novotny et al. (2001), (see also Fig. 3), which have been previously tested and proved adequate for most paths in the Aegean Sea (Benetatos et al., 2002, 2005). Original waveforms were cut into segments long enough to ensure resolution of

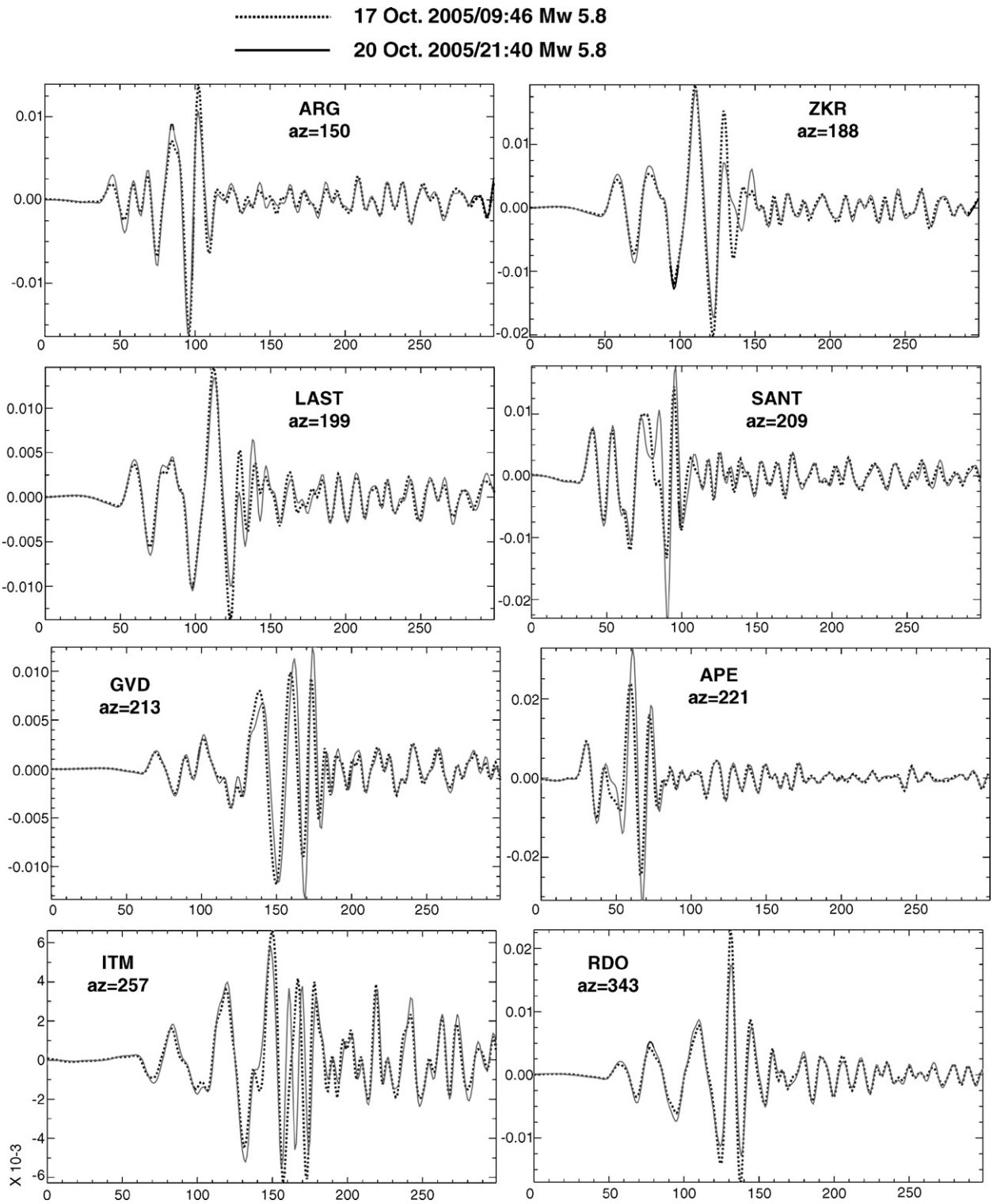

Fig. 6. Broad band records at stations (shown in Fig. 3) for the two strongest Mw 5.8 events of 17 October 2005 (09:46 UTC) (dashed lines) and of 20 October 2005 (21:40 UTC) (straight lines). All records are filtered between 0.02 and 0.1 Hz. The similarity of waveforms is striking both in shape and amplitude which favours their close location in space, their magnitude equality, and their focal mechanism similarity that we obtained. The comparison to the waveforms of the first Mw 5.4 was not as good, implying a different location and mechanism.

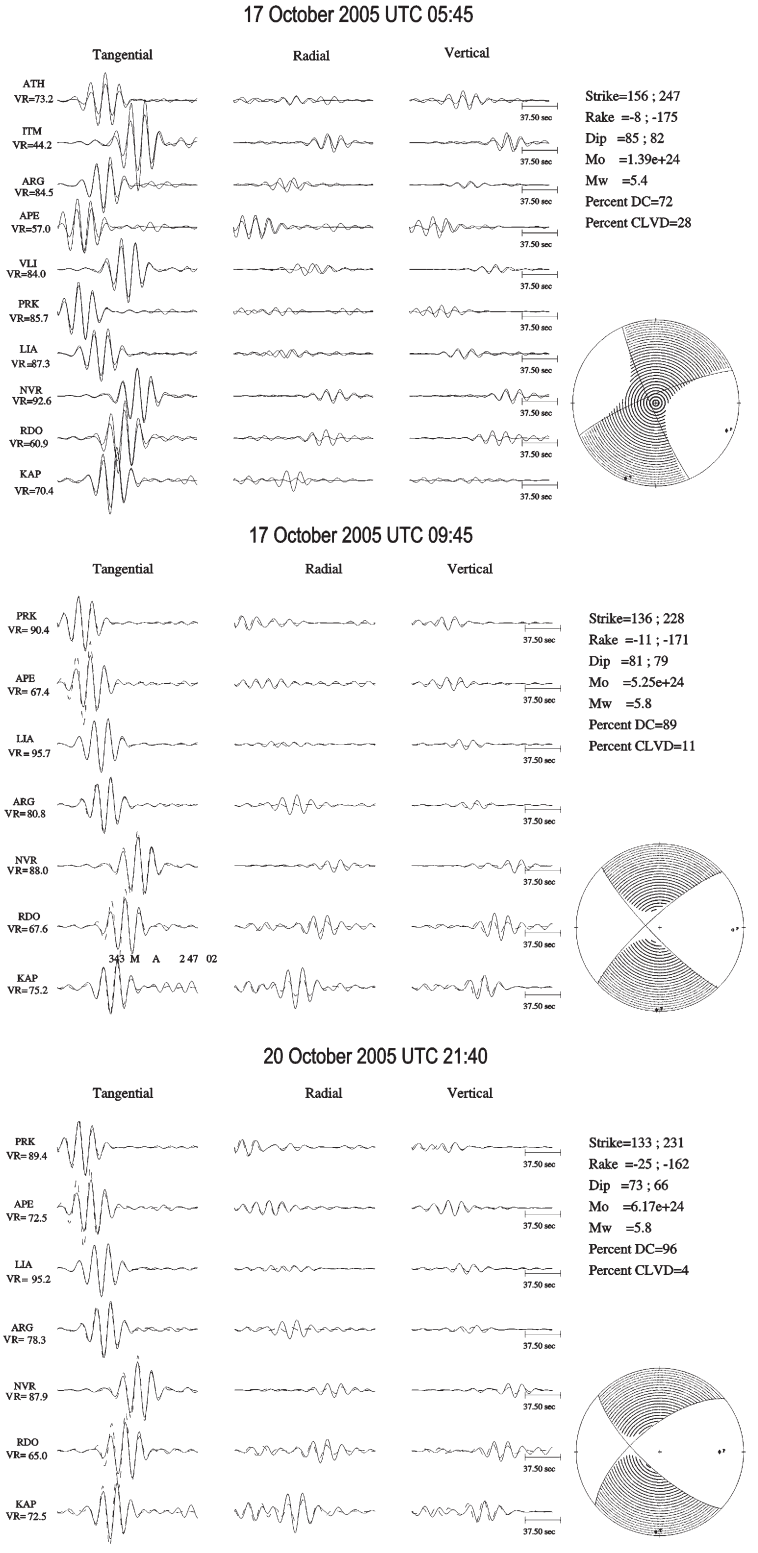

Fig. 7. Moment tensor inversion results (dashed line = synthetics, continuous lines = observed waveforms) obtained for the three strongest events of the sequence as marked. On the left part the variance reduction is presented for each station and on the right part the strike, dip and rake of the solution along with the seismic moment and the percentage of double couple (DC) and the percentage of the Compensated Linear Vector Dipole (CLVD).

the low frequencies, carefully examined to enclose only one event in each data segments and avoid interference between two or more consequently earthquakes that occurred very close in time. Then, the waveforms were corrected for the instrument response, re-sampled at a sampling rate of 1 Hz, integrated to displacement and pass band filtered between 0.05 and 0.08 Hz. For smaller magnitude events we sometimes filtered between 0.05 and 0.1 Hz to allow for higher frequencies. The optimum depth for each event was found with a grid search (in the range of 2 to 30 km with a step of 2 km) and the selection was based on the variance reduction that the inversion routine was returning at each run and the percent double couple of the focal mechanism. We expect from a reliable solution to have high variance reduction and high percentage of double couple force acting at the source. The focal mechanism solutions proved to be stable during the tests at different depths (we indicatively show in Fig. 7 the solutions for the three strongest events), although it was necessary in many cases to manually align the synthetics relative to the observed waveforms in order to achieve the best fit. When a satisfactory solution was obtained we were refining our depth search with a step of 1 km. The method of moment tensor inversion can be used with single station records (Dreger, 2002). We tested this, for

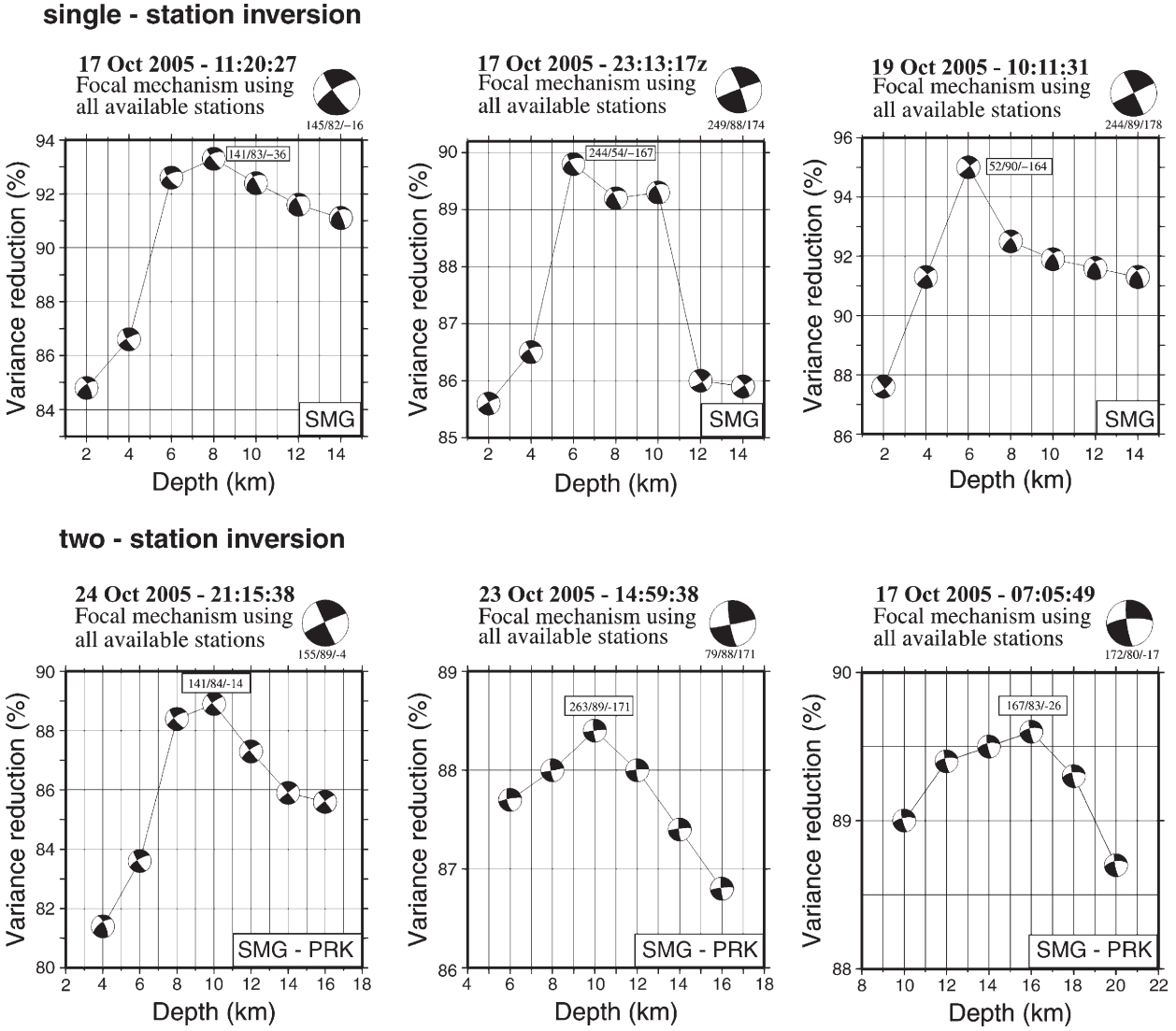

Fig. 8. Examples of single (SMG) and two-station inversion (SMG and PRK) in order to show the stability of the focal mechanism when using few stations. At the upper part of each plot the focal mechanism obtained with all available stations is presented and just below the focal mechanism using SMG or SMG and PRK for various depths with its corresponding variance reduction (VR%).

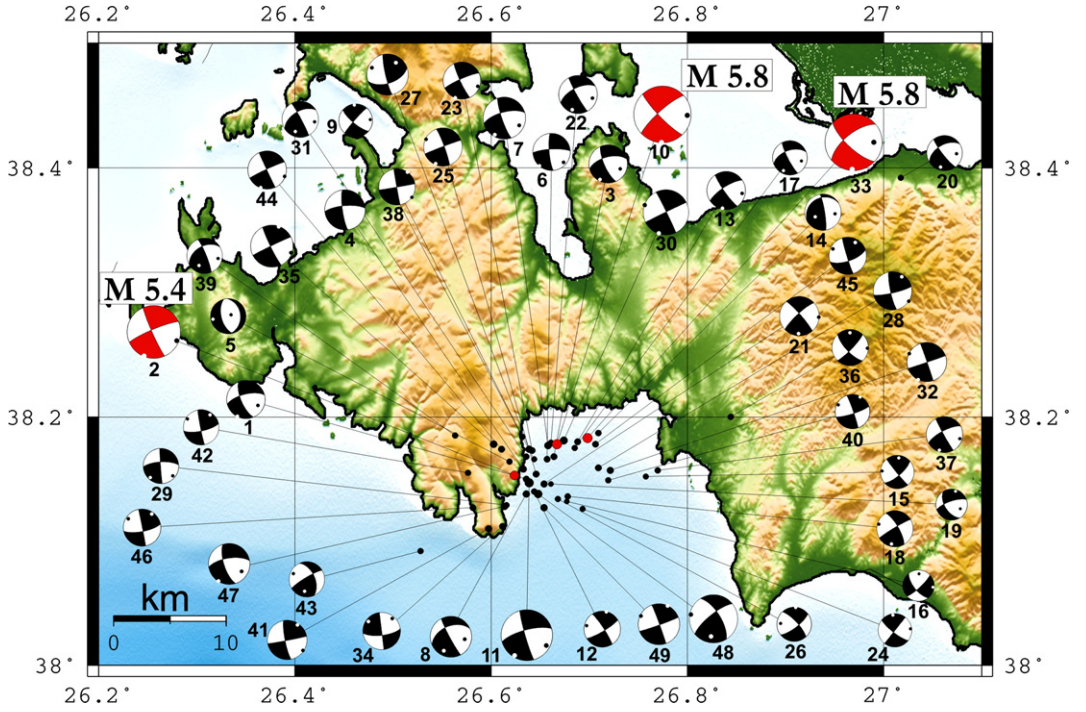

Fig. 9. Distribution of the focal mechanisms here determined (numbers as in Table 2). The operation of steeply dipping strike-slip faulting in the region is evident.

six earthquakes, using only one or two close stations (SMG or SMG and PRK). In all cases the similarity of our final solution with the one obtained using single or two stations records in the inversion was proved (Fig. 8). Moreover, from the stations used in the inversions (Fig. 3), SMG and PRK at distances of 50 km and 125 km, respectively from the centre of the seismic sequence, provided very stable solutions, further validating the velocity model used.

Earthquake focal mechanisms (Table 2 for parameters) with magnitudes ranging from $3.2 \leq Mw \leq 5.8$, clearly show (Fig. 9) extensive strike-slip motions along the entire activated area. The average P axis trends at N104±22° E and the average T-axis trends at N200±24° E in accordance with the regional stress field (Kiratzi, 2002; Kiratzi and Louvari, 2003). Strike-slip motions were also observed by Melis and Konstantinou (2006) in a set of 15 focal mechanisms of the sequence that they determined applying moment tensor inversion.

4. Coseismic Coulomb stress changes

Strong earthquakes can trigger earthquakes at short distances from the epicentre by transferring static or dynamic stresses (e.g. Harris et al., 1995; Caskey and Wesnousky, 1997; Harris and Simpson, 1998; Gomberg et al., 2001; Ganas et al., 2005a). The earthquake induced stress changes are applied to neighbouring receiver faults (as termed in Reasenberg and Simpson, 1992) using the Coulomb Failure Function:

$$\Delta CFF = \Delta\tau + \mu'(\Delta\sigma_n) \quad (1)$$

where $\Delta\tau$ is the coseismic change in shear stress on the receiver fault and in the direction of fault slip, $\Delta\sigma_n$ is the

Table 3
Slip models for the source faults of the three strongest events used in the stress changes calculations

#	Event name; Time	Epicentre Lon° N, Lat° E	Length (km)	Width (km)	Strike (°)	Dip (°)	Rake (°)	U_s (m)	U_d (m)	Mw
1	17.10.2005; 05:45 UTC	38.153, 26.620	6	5	247	82	−175	−0.139	0.012	5.4
2	17.10.2005; 09:46 UTC	38.178, 26.663	10	6	228	79	−171	−0.275	0.043	5.8
3	20.10.2005; 21:40 UTC	38.183, 26.694	10	6	231	66	−162	−0.264	0.086	5.8

Fault length and width according to Wells and Coppersmith (1994). U_s and U_d are the average strike-slip component and the average dip slip component, respectively.

Table 4
Input parameters used for stress transfer modelling

Poisson's ratio	0.25
Shear modulus, μ	3×10^{10} Pa (3×10^{5} bars)
Map projection	UTM zone 35
Depth of ΔCFF calculation	7 km (Fig. 10), 12 km (Fig. 11)
Grid size	1 km
Effective Friction Coefficient (μ')	0.4 (based on Harris and Simpson, 1998).
Target (Receiver) Planes: NE–SW trending associated with right lateral strike-slip motion	
Strike/dip angle-direction/rake	228/79NW/-171

change in normal stress acting on the receiver fault (with tension positive), and μ' is the effective coefficient of friction,

$$\mu' = \mu(1-\Delta p/\Delta\sigma_n) \quad (2)$$

where μ is the static coefficient of friction and Δp is the pore pressure change within the fault.

To resolve stress on individual fault planes we used the code DLC (written by R. Simpson, based on the subroutines of Okada (1992)), to calculate changes in the stress tensor at points along a specified receiver fault surface caused by slip on a source fault in an elastic half space. Table 3 summarizes the fault slip models we use (as previously obtained) extending from mid-upper crustal levels to a depth of 15 km and Table 4 gives the values of the parameters used for the stress change calculations. All source faults are modelled as, oblique-slip, inclined rectangular dislocations, ignoring local fault complexities.

At first we evaluated the triggering capability of the source fault of the first Mw 5.4 event (17-10-2005 05:45 UTC), and we calculated the amount of Coulomb stress which was transferred to the region of occurrence of the 17-10-2005 and 20-10-2005 events. The target (receiver) planes are dextral strike-slip faults with slip models identical to that of the 17-10-2005 09:46 UTC. We sampled ΔCFF (Coulomb stress change between the initial stress and the final stress) on a horizontal section at 7 km depth on a 100×100 km grid surrounding the source event epicentre, with 1 km grid spacing. The depth of horizontal plane was chosen to comply with the hypocentre depth of the two Mw5.8 events of 17 October and 20 October 2005. We used the program ELFGRID to calculate the stress tensor grid at 7 km depth. Then we applied the program STROP which uses that tensor to calculate the tractions at that depth on planes of specified orientation. STROP outputs a ΔCFF file that does the calculation in Eq. (1) above on the planes of interest for the friction value specified. We interpret a positive value of ΔCFF to indicate that a fault plane occurring within this stress lobe has been brought closer to failure; when ΔCFF is negative, the fault is brought further from failure (i.e. relaxed).

For the Mw 5.4 event and its triggering capability we used this method to additionally examine if the NE–SW plane is the fault plane, further to support our directivity observations. Thus, we examined two source models, at two different depths (considering the uncertainty in the depth estimate): a) a NW–SE trending rupture plane associated with left lateral strike-slip motion at a depth of 10 km (Fig. 10a) and of 15 km (Fig. 10b) and b) a NE–SW trending rupture associated with right lateral strike-slip motion at a depth of 10 km (Fig. 10c) and of 15 km (Fig. 10d). Both models predict that the epicentres of two Mw 5.8 events are in the regions where stress was transferred. The shallower sources (10 km) for the Mw 5.4 event predict positive stress levels ΔCFF < 0.25 bars for a NW–SE trending plane (Fig. 10a) whereas for a NE–SW trending plane the loading levels are considerably larger and of the order of 0.25 to 0.75 bars (Fig. 10c). This is an indication for the operation of the NE–SW plane, but not strong evidence, taking into account that ΔCFF levels > 0.1 bar are associated with earthquake triggering on neighbouring faults (Harris et al., 1995) and that a triggering threshold has not yet been established (e.g. Ziv and Rubin, 2000). For the deeper sources (at 15 km depth) the stress loading levels (Fig. 10b, d) are smaller by a factor of three, as compared to the shallow sources. The hypocentre depth of the Mw 5.4 event is crucial for the triggering hypothesis if a triggering threshold exists at ~+0.1 bars, that is why we examined ΔCFF at two depth ranges. From the rupture models examined for the first event we prefer the one of NE–SW rupturing (Fig. 10c), because it is in accordance with the directivity pattern, the

Fig. 10. Coulomb stress changes at 7-km depth associated with the 17-10-2005 (05:45 UTC); Mw 5.4 earthquake. Palette of stress values is linear in the range −2 to +2 bar. White colour indicates area where transferred stress >2 bar and black colour the area where stress reduction was >−2 bar. Stars show the three mainshock epicentres and ellipses their estimated location error. Target fault planes are also shown as straight lines. Blue areas indicate unloading, red areas indicate loading, respectively. Effective coefficient of friction is 0.4 in all cases. Slip models are shown in Table 3. Colour scale in bar (1 bar = 100 KPa). a) Source slip model assuming rupture of a NW–SE plane with sinistral strike-slip motion at a hypocentre depth of 10 km; b) as in a) but at a hypocentre depth of 15 km; c) Source slip model assuming rupture of a NE–SW plane with dextral strike-slip motion at a hypocentre depth of 10 km; d) as in c) but with hypocentral depth at 15 km. In b) and d) note the reduction of transferred stress near the two strongest Mw 5.8 epicentres by a factor of three.

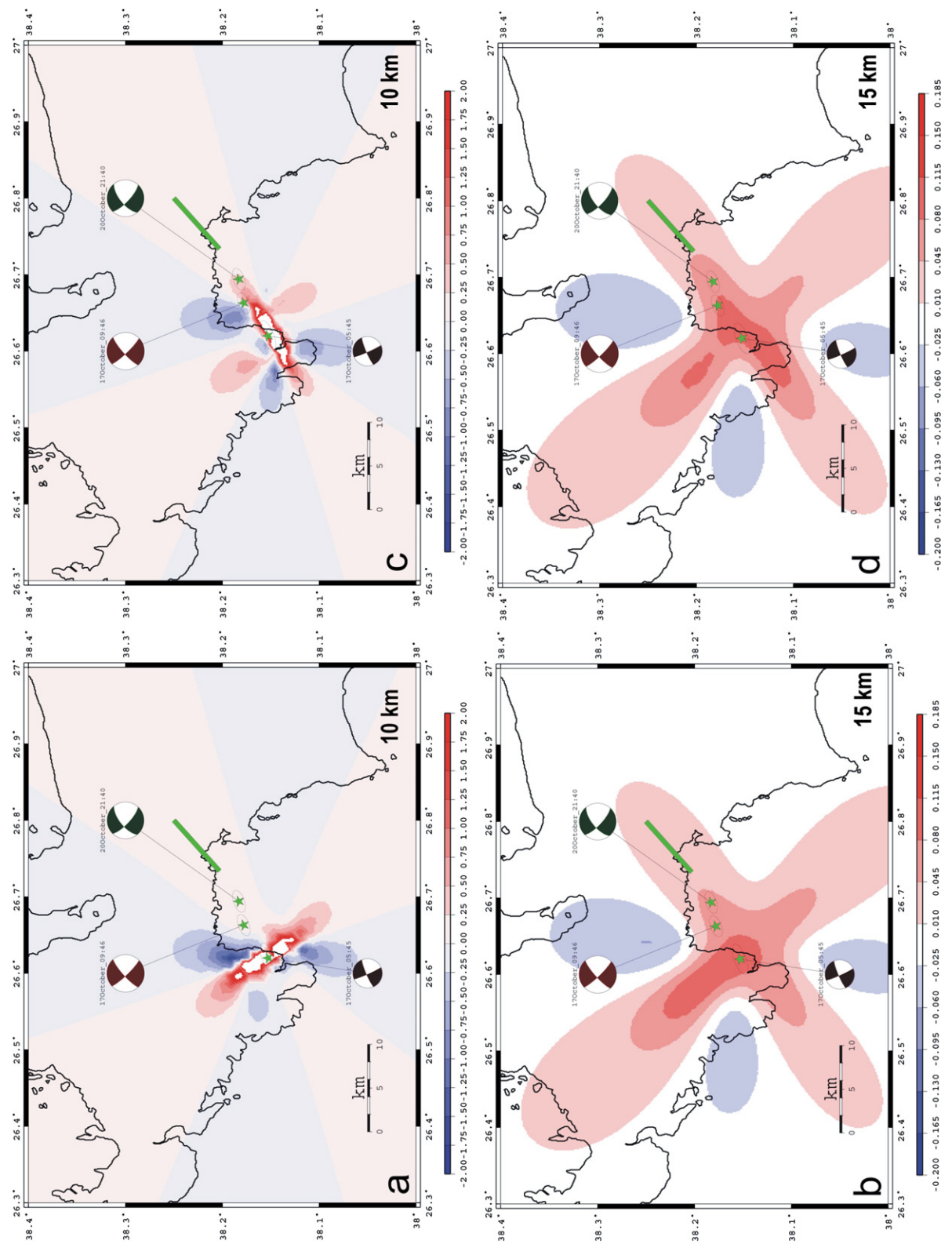
a
10 km
b
15 km
c
10 km
d
15 km
17October 09:46
17October 05:45
20October 21:40
km
0 5 10
-2.00 -1.75 -1.50 -1.25 -1.00 -0.75 -0.50 -0.25 0.00 0.25 0.50 0.75 1.00 1.25 1.50 1.75 2.00
-0.200 -0.165 -0.130 -0.095 -0.060 -0.025 0.010 0.045 0.080 0.115 0.150 0.185

distribution of aftershocks, and it clearly predicts that the epicentres of the two Mw 5.8 events, taking into account their epicentre uncertainties, are clearly in the regions where stress was most increased.

We have to comment that, as the epicentre of the 20.10.2005 Mw 5.8 event is located 2.7 km to the east of the 17.10.2005 Mw 5.8 event, our static stress transfer modelling could not document triggering because this area is relaxed after the combined stress field calculations of the first two events. Perhaps the uniform-slip model adopted here is inadequate to simulate the actual rupture process and associated stress transfer in this case because slip irregularities can cause local peaks in stress. However, we note that a positive lobe where $\Delta CFF > 1$ bar exists 2 km to the east of the error margin of the 20.10.2005 epicentre, no matter which rupture combination we adopt for the first two events.

Fig. 11 shows the stress change throughout the crust, combining the effects of the three strongest events of the sequence (Table 3), along planes oriented to maximize the Coulomb stress change (Stein et al., 1992), at a depth of 12 km (average depth of all aftershocks that we analysed). For the calculations we assume the regional stress field at 200 bars (20 MPa) consisting of uniaxial E–W compression (*T*-axis azimuth at N200° E). The theoretical optimal failure angle for a horizontal axis of maximum compression is 34.1° for $\mu' = 0.4$. Coulomb stress increase of ~5 bars is predicted in lobes following a NE–SW trend, well explaining the occurrence of the two strongest events. We also observe that there is a satisfactory, positive correlation between sites of aftershocks and stress increase. Many aftershocks were triggered at distances of 20–30 km away from the Gulf of Sığaçik where $\Delta CFF < 0.5$ bar. The "stress shadow" effect is also visible to the north and to the

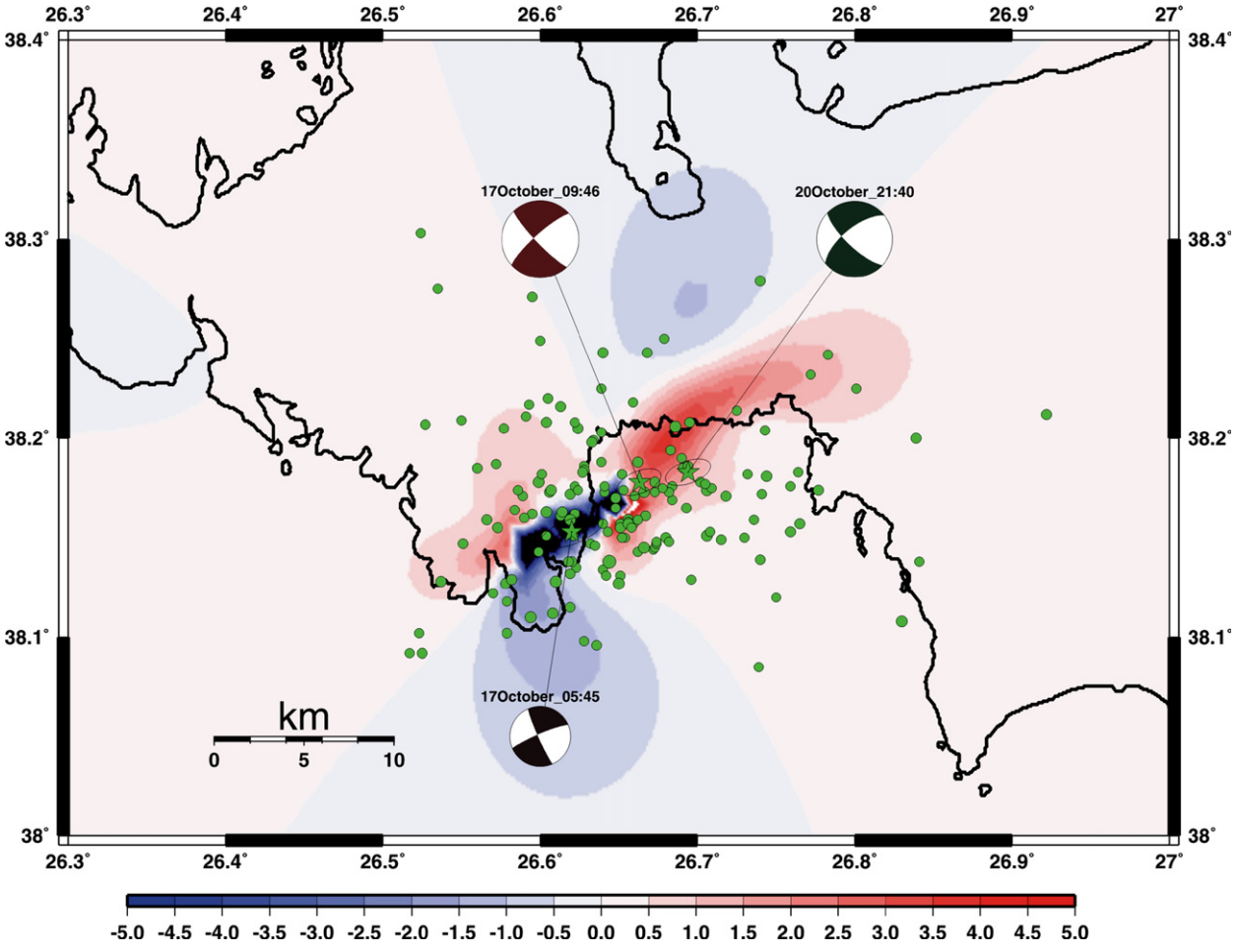

Fig. 11. Stress change calculated on optimal planes to regional compression (remote stress at 200 bars). Palette of stress values is linear in the range −5 to +5 bar. Blue areas indicate unloading, red areas indicate loading, respectively. Circles represent aftershocks after 20 October 2005 (21:40 UTC). The occurrence of the two Mw5.8 events is well documented in the loaded regions.

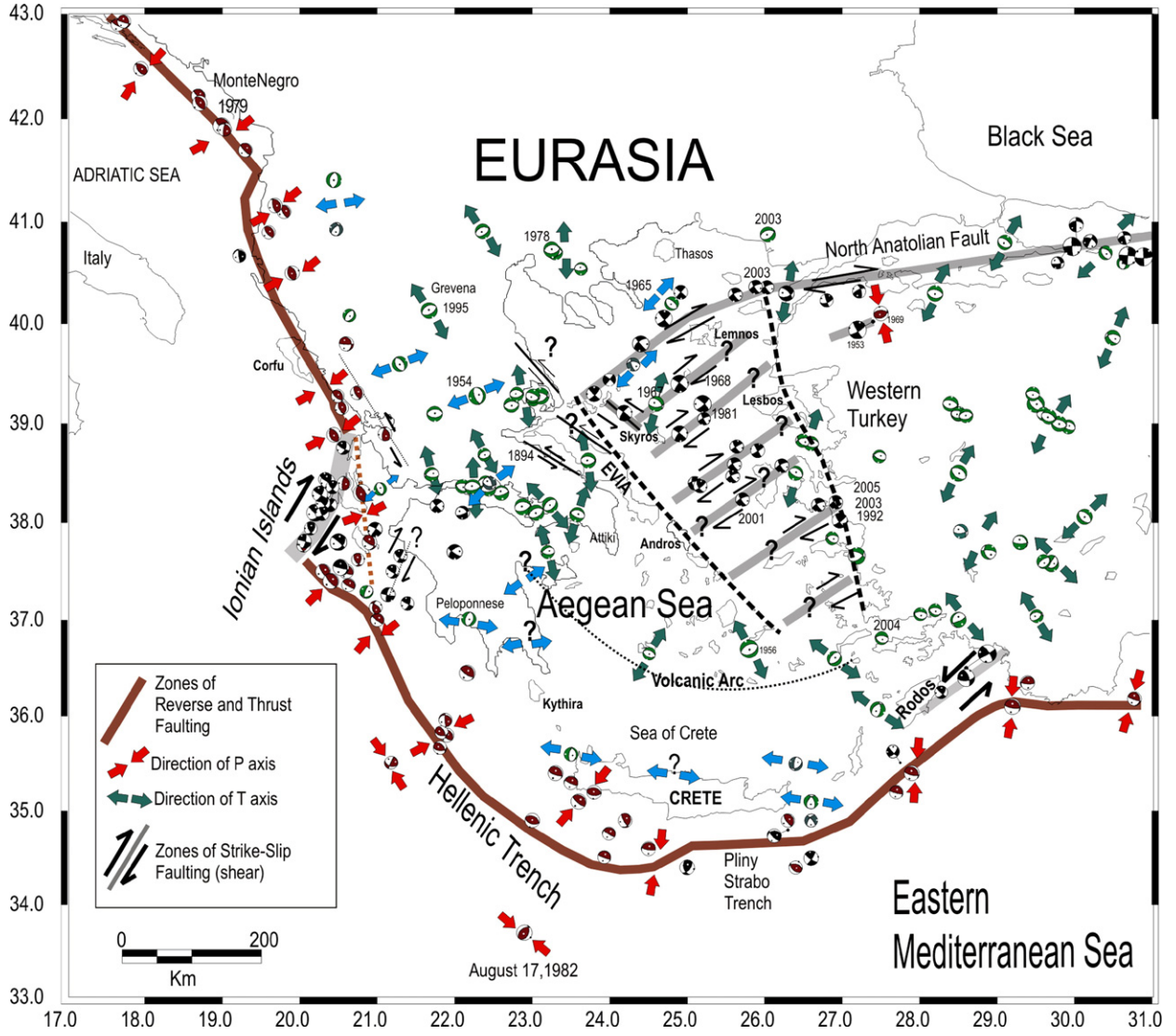

Fig. 12. Map showing the orientation of *P* and *T* axes in the Aegean Sea and the surrounding lands. Focal mechanisms are also plotted with beach-ball sizes that scale with earthquake magnitude. Note the distributed strike-slip motions in the central Aegean Sea that facilitate the transfer of Anatolia motion to the normal faulting system of continental Greece. The question marks denote areas, which still lack focal mechanisms and where future data are expected to shed light on the seismotectonics (figure modified from Kiratzi and Louvari, 2003).

south of the Gulf of Siğaçik where $\Delta CFF < -1.5$ bar. A few aftershocks occur inside these relaxed areas and within a distance of <10 km from the epicentres of the three strongest events. We infer that our stress change calculations have been adequately validated by the observed distribution of aftershocks.

5. Discussion and conclusions

The moderate-size earthquake sequence of October 2005 occurred in western Turkey (Gulf of Siğaçik) close to the Greek islands of Samos and Chios. The sequence is interesting because it indicates rupture of dextral strike-slip faults in a region dominated by ~ N–S extension and well developed mainly east-west trending normal faults. Three were the strongest events of the sequence. The first Mw 5.4 event occurred on 17 October 2005 (05:45 UTC) at the western tip of Gulf of Siğaçik, and was followed 4 h later (09:46 UTC) by an Mw 5.8 event, and 3 days later, on 20 October by another Mw 5.8 event, both occurring to the east of the first event, along the central part of Siğaçik Gulf.

We combined phases from the Greek and Turkish networks to relocate more than 200 aftershocks. A general

alignment of the best located epicentres along a general NE–SW trend is observed, however a characteristic of this sequence is the considerable spread of aftershocks implying simultaneous activation of other structures in the region that mainly have a NW–SE trend (also observed by Aktar et al., submitted for publication), resembling the compound earthquake sequence that occurred in November 1987, near Superstition Hills in California (Hudnut et al., 1989; Scholz, 1994). Such a complex fault structure has been identified in this area on the basis of reflection data (Ocakoğlu et al., 2004, 2005 and references therein). Moreover, the presence of geothermal fields in the region (Drahor and Berge, 2006), and the unstable condition of the fault systems they imply, probably explains the diffuse pattern of aftershock activity off the main rupture, shortly after the occurrence if the first two strong events.

We used moment tensor inversion applied to regional broad band records to determine the focal mechanisms of 49 events of the sequence. All (except one) of the focal mechanisms are connected with pure strike-slip motions along very steep planes, extending in depth from 4 km to 22 km.

Based on the similarity of waveforms, the distribution of aftershocks, the clear directivity towards ENE of the first event (Benetatos et al., 2006 in preparation), the stress transfer analysis and the previous knowledge of regional tectonics we conclude that all three strongest events of the 2005 sequence ruptured a steeply dipping right lateral strike-slip fault trending NE–SW with an average mechanism of strike 235°, dip 75° and rake −170°. The event propagation towards east is well explained by the stress transfer modelling.

Fig. 12 presents the distribution of focal mechanisms in the broader Aegean Sea area from a database we constantly update (figure modified from Kiratzi and Louvari, 2003), together with the direction of *P* and *T* axes. If we focus our attention in the central Aegean Sea, north of the volcanic arc, we observe that as new data are collected there is evidence of distributed strike-slip motions along mainly NE–SW striking planes exhibiting right lateral sense of motion. This distributed strike-slip faulting, with slip vectors parallel to the GPS vectors, facilitates the westward motion of Anatolia plate. These strike-slip faults often sub-parallel, operate as transfer fault systems that connect two extensional regimes: the extensional regime of western Anatolia, in the east, and the extensional regime of continental central Greece, in the west. In this pattern the existence of NW–SE striking strike-slip faults is also evident. Evidence for the operation of this NW–SE striking sinistral strike -slip faults in the Aegean Sea was first derived from the occurrence of the July 2001 sequence, north of Skyros Island (Roumelioti et al., 2003, 2004; Ganas et al., 2005b). The sequence studied here, intensifies the operation of strike-slip faulting in the central Aegean Sea–western Turkey, in regions that are well-away from the North Anatolian Fault system, indicating that strike-slip motions are the most optimal to the stress-field to transfer the motion from Anatolia into continental Greece.

Acknowledgments

Thanks are due to two anonymous reviewers and the editor for their constructing comments. Dogan Kalafat, from Kandilli Observatory, is gratefully thanked for his immediate response in providing phase data from the Turkish network. We also thank our friends and colleagues Mustafa Aktar, and Hayrullah Karabulut, from Kandilli Observatory, for providing results prior to publication and useful discussions. George Karakaisis and Spyros Pavlides, from the Department of Geology of the Aristotle University of Thessaloniki, are also thanked for stimulating discussions. This work was financed in part by the General Secretariat of Research and Technology (Ministry of Development) of Greece and in part (C.B.) by the Ministry of Education and Religious Affairs (Project Pythagoras II). Most of the figures were plotted using the GMT software (Wessel and Smith, 1995). The software RAKE (Louvari and Kiratzi, 1997) was also used to handle the focal mechanism database.

References

Aktar, M., Karabulut, H., Ozalaybey, S., Childs, D.M., submitted for publication. A conjugate strike-slip fault system within the extensional tectonics of western Turkey.

Altinok, Y., Alpar, B., Özer, N., Gazioglu, C., 2005. 1881 and 1949 earthquakes at the Chios–Cesme Strait (Aegean Sea) and their relation to tsunamis. Nat. Hazards Earth Syst. Sci. 5, 717–725.

Benetatos, C., Roumelioti, Z., Kiratzi, A., Melis, N., 2002. Source parameters of the M 6.5 Skyros island (North Aegean Sea) earthquake of July 26, 2001. Ann. Geophys. 45, 513–526.

Benetatos, Ch., Kiratzi, A., Roumelioti, Z., Stavrakakis, G., Drakatos, G., Latoussakis, I., 2005. The 14 August 2003 Lefkada Island (Greece) earthquake: focal mechanisms of the mainshock and of the aftershock sequence. J. Seismol. 9, 171–190.

Caskey, S.J., Wesnousky, S.G., 1997. Static stress changes and earthquake triggering during the 1954 Fairview peak and Dixie valley earthquakes, central Nevada. Bull. Seismol. Soc. Am. 87 (3), 521–527.

Dewey, J.F., Sengör, A.M.C., 1979. Aegean and surrounding regions: complex multiple and continuum tectonics in a convergent zone. Geol. Soc. Amer. Bull. 90, 84–92.

Drahor, M., Berge, M., 2006. Geophysical investigations of the Seferihisar geothermal area, western Anatolia, Turkey. Geothermics 35, 302–320.

Dreger, D., 2002. Manual of the Time-Domain Moment Tensor Inverse Code (TDMT_INVC), Release 1.1. Berkeley Seismological Laboratory, p. 18.

Dreger, D., Helmberger, D., 1990. Broadband modelling of local earthquakes. Bull. Seismol. Soc. Am. 80, 1162–1179.

Dreger, D., Helmberger, D., 1991. Complex faulting deduced from broadband modelling of the 28 February 1990 Upland earthquake (ML=5.2). Bull. Seismol. Soc. Am. 81, 1129–1144.

Dreger, D., Helmberger, D., 1993. Determination of source parameters at regional distances with single station or sparse network data. J. Geophys. Res. 98, 8107–8125.

Ganas, A., Shanov, S., Drakatos, G., Dobrev, N., Sboras, S., Tsimi, C., Frangov, G., Pavlides, S., 2005a. Active fault segmentation in southwest Bulgaria and Coulomb stress triggering of the 1904 earthquake sequence. J. Geodyn. 40 (2–3), 316–333.

Ganas, A., Drakatos, G., Pavlides, S., Stavrakakis, G., Ziazia, M., Sokos, E., Karastathis, V., 2005b. The 2001 Mw=6.4 Skyros earthquake, conjugate strike-slip faulting and spatial variation in stress within the central Aegean Sea. J. Geodyn. 39, 61–77.

Gomberg, J., Reasenberg, P.A., Bodin, P., Harris, R.A., 2001. Earthquake triggering by seismic waves following the Landers and Hector Mine earthquakes. Nature 411, 462–466.

Harris, R., 1998. Introduction to special section: stress triggers, stress shadows, and implications for seismic hazard. J. Geophys. Res. 103, 24,347–24,358.

Harris, R.A., Simpson, R.W., 1998. Suppression of large earthquakes by stress shadows: a comparison of Coulomb and rate-and-state failure. J. Geophys. Res. 103, 24439–24451.

Harris, R.A., Simpson, R.W., Reseanberg, P.A., 1995. Influence of static stress changes on earthquake locations in southern California. Nature 375, 221–224.

Hudnut, K.W., Seeber, L., Pacheco, J., 1989. Cross-fault triggering in the November 1987 Superstition Hills earthquakes sequence, Southern California. Geophys. Res. Lett. 16, 199–202.

Kiratzi, A., 2002. Stress tensor inversions along the westernmost north and central Aegean Sea. Geophys. J. Int. 106, 433–490.

Kiratzi, A., Louvari, E., 2003. Focal mechanisms of shallow earthquakes in the Aegean Sea and the surrounding lands determined by waveform modelling: a new database. J. Geodyn. 36, 251–274.

Koukouvelas, I., Aydin, A., 2002. Fault structure and related basins of the North Aegean Sea and its surroundings. Tectonics 21 (5), 1046, doi:10.1029/2001TC901037.

Lahr, J.C., 1999. HYPOELLIPSE: A Computer Program for Determining Local Earthquake Hypocentral Parameters, Magnitude and First-Motion Pattern, Y2K Version, USGS Open-File Report 99-23.

Louvari, E., Kiratzi, A., 1997. Rake: a Window's program to plot earthquake focal mechanisms and stress orientation. Comput. Geosci. 23, 851–857.

McClusky, S., Balassanian, S., Barka, A., Demir, C., Georgiev, I., Hamburg, M., Hurst, K., Kahle, H., Kastens, K., Kekelidze, G., King, R., Kotzev, V., Lenk, O., Mahmoud, S., Mishin, A., Nadariya, M., Ouzounis, A., Paradissis, D., Peter, Y., Prilepin, M., Reilinger, R., Sanli, I., Seeger, H., Tealeb, A., Toksoz, M.N., Veis, G., 2000. Global Positioning System constraints on plate kinematics and dynamics in the eastern Mediterranean and Caucasus. J. Geophys. Res. 105, 5695–5720.

Melis, N., Konstantinou, K., 2006. Real-time seismic monitoring in the Greek region: an example from the 17 October 2005 east Aegean Sea earthquake sequence. Seismol. Res. Lett. 77, 364–370.

Novotny, O., Zahradnik, J., Tselentis, G.-A., 2001. North-western Turkey earthquakes and the crustal structure inferred from surface waves observed in Western Greece. Bull. Seismol. Soc. Am. 91, 875–879.

Ocakoğlu, N., Demirbağ, E., Kuşçu, İ., 2004. Neotectonic structures in the area off shore of Alaçati, Doğanbey and Kuşadasi (western Turkey): evidence of strike-slip faulting in the Aegean extensional province. Tectonophysics 391, 67–83.

Ocakoğlu, N., Demirbağ, E., Kuşçu, İ., 2005. Neotectonic structures in İzmir Gulf and surrounding regions (western Turkey): evidences of strike-slip faulting with compression in the Aegean extensional regime. Mar. Geol. 219, 155–171.

Okada, Y., 1992. Internal deformation due to shear and tensile faults in a half-space. Bull. Seismol. Soc. Am. 82, 1018–1040.

Panagiotopoulos, D., 1984. Travel time curves and crustal structure in the southern Balkan region. PhD thesis, University of Thessaloniki, 159 pp. (in Greek).

Papazachos, C.B., 1999. Seismological and GPS evidence for the Aegean–Anatolia interaction. Geophys. Res. Lett. 26 (17), 2653–2656.

Papazachos, B.C., Papazachou, C., 2002. The Earthquakes of Greece. Ziti Publ., Thessaloniki, Greece. 317 pp.

Reasenberg, P.A., Simpson, R.W., 1992. Response of regional seismicity to the static stress change produced by the Loma Prieta earthquake. Science 255, 1687–1690.

Roumelioti, Z., Kiratzi, A., Melis, N., 2003. Relocation of the July 26, 2001 Skyros Island (Greece) earthquake sequence using the double-difference technique. Phys. Earth Planet. Inter. 138, 231–239.

Roumelioti, Z., Kiratzi, A., Dreger, D., 2004. The source process of the July 26, 2001 Skyros Island (Greece) earthquake. Geophys. J. Int. 156 (3), 541–548.

Saikia, C.K., 1994. Modified frequency-wavenumber algorithm for regional seismograms using Filon's quadrature; modelling of Lg waves in eastern North America. Geophys. J. Int. 118, 142–158.

Scholz, C., 1994. The Mechanics of Earthquakes and Faulting. Cambridge Univ. Press, p. 439.

Scordilis, E., Kiratzi, A., Panagiotopoulos, D., 1994. A study of the earthquake of November 6, 1992 in Izmir (Turkey). Bull. Geol. Soc. Greece XXX/5, 243–249.

Stein, R.S., King, G., Lin, J., 1992. Change in failure stress on the southern San Andreas fault system caused by the 1992 Magnitude=7.4 Landers earthquake. Science 258, 1328–1332.

Wells, D.L., Coppersmith, K.J., 1994. New empirical relationships among magnitude, rupture length, rupture width, rupture are, and surface displacement. Bull. Seismol. Soc. Am. 84, 974–1002.

Wessel, P., Smith, W.H.F., 1995. New version of the Generic Mapping Tools released. Eos, Trans. - Am. Geophys. Union 76, 329.

Yilmaz, Y., 1997. Geology of Western Anatolia. In: Schindler, C., Pfister, M. (Eds.), Active Tectonics of NW Anatolia — the Marmara Poly-Project. VDF, ETH, Zurich.

Ziv, A., Rubin, A.M., 2000. Static stress transfer and earthquake triggering: no lower threshold in sight? J. Geophys. Res. 105 (B6), 13631–13642.